



Simple technique of determining the fibre diameter during etching

MEDYA F. NAMIQ^{1,2,*} AND MORTEN IBSEN¹

¹*Optoelectronics Research Centre, University of Southampton, SO17 1BJ, UK*

²*Ocean Technology and Engineering, National Oceanography Centre, SO14 3ZH, UK*

**M.F.N.Namiq@soton.ac.uk*

Abstract: We present a technique to measure, in situ, the diameter of an optical fibre during etching using a fibre Bragg grating (FBG). Differential shifts between the fundamental mode, and the higher-order Bragg resonances generated by the etching process are used to determine the diameter of a standard optical fibre (SMF28) with a precision of $\sim 200\text{nm}$. Numerical simulations are also carried out to investigate the overlap of the evanescent field of the fundamental mode and higher-order modes (LP11, LP02, LP21 and LP12). These simulations were used to find and calibrate the diameter of the etched-cladding fibre. Subsequently, the technique was used to experimentally determine the refractive index of two buffered hydrofluoric (BHF) acid solutions, (20:1) and (7:1), to be $\sim 1.360 \pm 0.005$ and $\sim 1.370 \pm 0.005$ respectively @ $\sim 1550\text{nm}$. The refractive index of both BHF solutions is calibrated against known indices of liquids and solvents, including deionised water, methanol, acetone, ethanol, isopropanol, and ethylene glycol. The numerical simulations and experimental results are in very good agreement. We believe the approach presented in this work provides a controlled technique to achieve precise target diameter of the etched fibres in real time.

© 2018 Optical Society of America under the terms of the [OSA Open Access Publishing Agreement](#)

1. Introduction

In the past two decades the uses of FBGs have expanded to cover a range of applications in part due to their simple concept, low insertion loss and compact design [1–16]. More specifically, optical sensing systems based on FBGs are now used in many aspects of detection – most typically of strain, temperature, and pressure [6,7], and they can be applied in harsh environments where traditional sensors fail [8,9]. Attention has increasingly focused on cladding-etched, or otherwise exposed core fibres such as microstructured FBG refractive index sensors because they can be designed to provide higher interaction with the surrounding environment. These sensors are based on increased evanescent field interaction with the measurand, and they have found implementations in, for example, chemical and biological fields to measure a variety of physical and chemical substance parameters, including various liquids, and gases [10–14]. Other implementations of these fibre optic sensors are based on coating the etched fibre cladding surface with materials such as carbon nanotubes (CNTs), Graphene oxides (GO), and gold [15–17]. In these implementations, the coating material interacts with the extended evanescent field leading to fibre sensors that provide much higher sensitivity than equivalent uncoated etched-FBGs such as it, for example, has been reported for a gas sensing application which showed a detection sensitivity of $\sim 0.2\text{ppm}$, and for a humidity sensing application which showed a sensitivity of $\sim 31\text{pm}/\%RH$ at $\lambda = 1550\text{nm}$ and 25°C [15–17]. In addition, other proposed functions based on etched-FBGs have also been investigated such as a tuneable filter where CNT was coated onto the surface of an etched FBG to utilize the optical absorption characteristic of CNTs to provide the wavelength tuning [18]. In that demonstration the Bragg wavelength of the etched FBG showed a tuning range against launched power of 2nm with a tuning rate of $0.026\text{nm}/\text{mW}$ [18].

In general, silica-based fibres are etched using hydrofluoric (HF) acid with concentrations ranging from pure HF (49%) to buffered HF (BHF) solutions, depending on the required

precision and final etch-quality of the fibre surface. Being able to precisely determine the final fibre diameter and thus evanescent field overlap with the measurand is vital, especially when seeking a high degree of precision and repeatability. Some applications require a very specific evanescent field overlap with the measurand, e.g. less than a percent in some instances, to better control and balance the losses of the manufactured devices (etched or tapered). In these cases, it is therefore essential to be able to precisely control the fibre diameter to ensure that the correct overlap has been achieved.

In the case where etching with HF is used as the means of achieving the reduced diameter, it is beneficial to also know the refractive index of the HF used in the etching process. There are several reports in literature on measuring the refractive index of HF acid by using Mach-Zehnder interferometric and reflectometric measurement techniques [10,19,20]. Previous work has also demonstrated fibre etching with HF to determine the fibre core diameter based on in situ monitoring of the shift of the Bragg wavelength of the fundamental mode (LP01) [21]. However, this concept was only reported for the case when the etching had reached the fibre core itself. In view of that, we explore this concept further, but through the observation of the higher-order mode resonances generated in the Bragg grating when the diameter is reducing with the aim of being able to determine the fibre diameter before the etching reaches the core, and thus better control the evanescent field overlap with a given measurand.

In this paper we demonstrate that the diameter of a cladding-etched FBG can be determined with a precision of $\pm 200\text{nm}$ even when the etching has not reached the core. The demonstration is based on the comparatively simple technique of measuring the relative shifts of the Bragg resonances between the fundamental mode LP01, and the higher-order modes, LP11, LP02, LP21 and LP12, generated when the fibre diameter is reducing during etching. The higher-order Bragg resonances manifest themselves, even in standard SMF28 fibres, when the diameter is around $\sim 25\mu\text{m}$ and below, albeit weakly, becoming gradually stronger as the diameter is reducing. Using this technique we demonstrate that the fibre diameter can be monitored, in real-time, with high precision during the final stages of the etching process to ensure that the desired diameter is reached for a given application.

2. Theoretical analysis and simulations

The main operating principle of a Bragg grating based sensor is that the Bragg wavelength λ_B is sensitive to changes in either the effective refractive index of the propagating mode n_{eff} and/or the pitch Λ of the grating [5].

$$\lambda_B = 2n_{eff}\Lambda \quad (1)$$

$$\frac{\Delta\lambda_B}{\lambda_B} = \frac{\Delta n_{eff}}{n_{eff}} + \frac{\Delta\Lambda}{\Lambda} \quad (2)$$

Fibre Bragg gratings based on single mode fibre supports only the fundamental mode, LP01, when operating above the fundamental cut-off wavelength of the fibre. However, the process of etching the fibre cladding results in a progressive change of the effective refractive index of the propagating mode due to an increasing mode confinement and numerical aperture (NA), prompting a shift in the reference Bragg wavelength λ_B . Ignoring temperature effects, this change can be expressed as,

$$\Delta\lambda_B = 2\Delta n_{eff}\Lambda \quad (3)$$

As the fibre is being etched the corresponding values of the normalized propagation constant b and V-number will also be different to that of the pristine fibre. This in turn implies that, at some stage when the V-number exceeds 2.405 the fibre can begin to support higher-order modes and therefore also, in the case when a Bragg grating is written in the fibre, to support higher-order Bragg resonances [22,23] as schematically illustrated in Fig. 1. Because of

different cut-off wavelengths of various modes in the fibre, the evanescent field values of the fundamental mode LP01 and the higher-order modes LP_{xy} will also be different. They are therefore also affected by the surrounding refractive index (RI) to a different extent. Consequently, the Bragg wavelength-shifts of these modes will be different, depending on the etched diameter of the FBG and the refractive index of the surrounding material. According to the Bragg resonance condition in Eq. (1), and therefore the Bragg wavelength change in Eq. (3), the relative shifts, $\Delta\lambda_{LPxy}$, between the fundamental mode LP01 and higher-order LP_{xy} modes can be expressed as,

$$\Delta\lambda_{LPxy} = 2(n_{eff}^{LP01} - n_{eff}^{LPxy})\Lambda \quad (4)$$

where n_{eff}^{LP01} and n_{eff}^{LPxy} are the effective refractive indices of the fundamental mode and the higher-order modes, respectively.

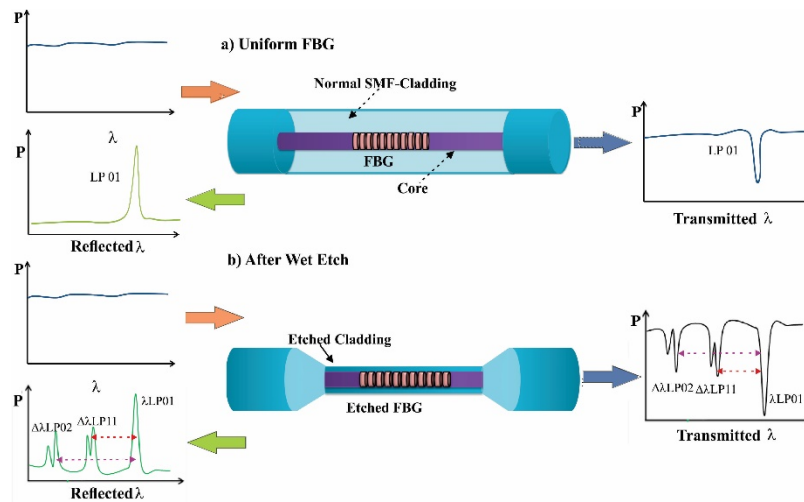


Fig. 1. Schematic representation of a Fibre Bragg grating before and after being cladding etched.

We investigate this principle numerically using the finite element based model COMSOL Multiphysics, to solve the wave equation and obtain the changes of the different effective mode-indices of the fundamental mode and higher order modes against a thinning fibre-cladding, and for various external refractive indices. The basic parameters of the simulated single mode fibre is based on those of the SMF28, i.e. core and initial cladding diameter values of 8.2 μ m and 125.0 μ m, respectively, and core and cladding refractive indices of 1.4489 and 1.4440, respectively @ ~1550nm. The model uses, NA = 0.119, V-number = 1.979, for a fibre cut-off wavelength of 1275.0nm.

3. Analysis of evanescent field overlaps of different generated modes

By applying the abovementioned model we analyse the fraction of modal power (FMP) extending beyond the fused silica cladding immediately surrounding the core (inner-cladding) into the outer-cladding (external layer surrounding the etched fibre cladding) in a single mode fibre with parameters as described above. Initially a refractive index of 1.3600 of the outer-cladding was investigated. As is evident from Fig. 2(b), 2(d) and 2(f), the first higher-order mode, LP11, unsurprisingly has a larger FMP value in the outer-cladding compared to the fundamental mode LP01 [Fig. 2(a), 2(c), and 2(e)], and thus the LP11 mode has a lower effective refractive index for a given fibre diameter.

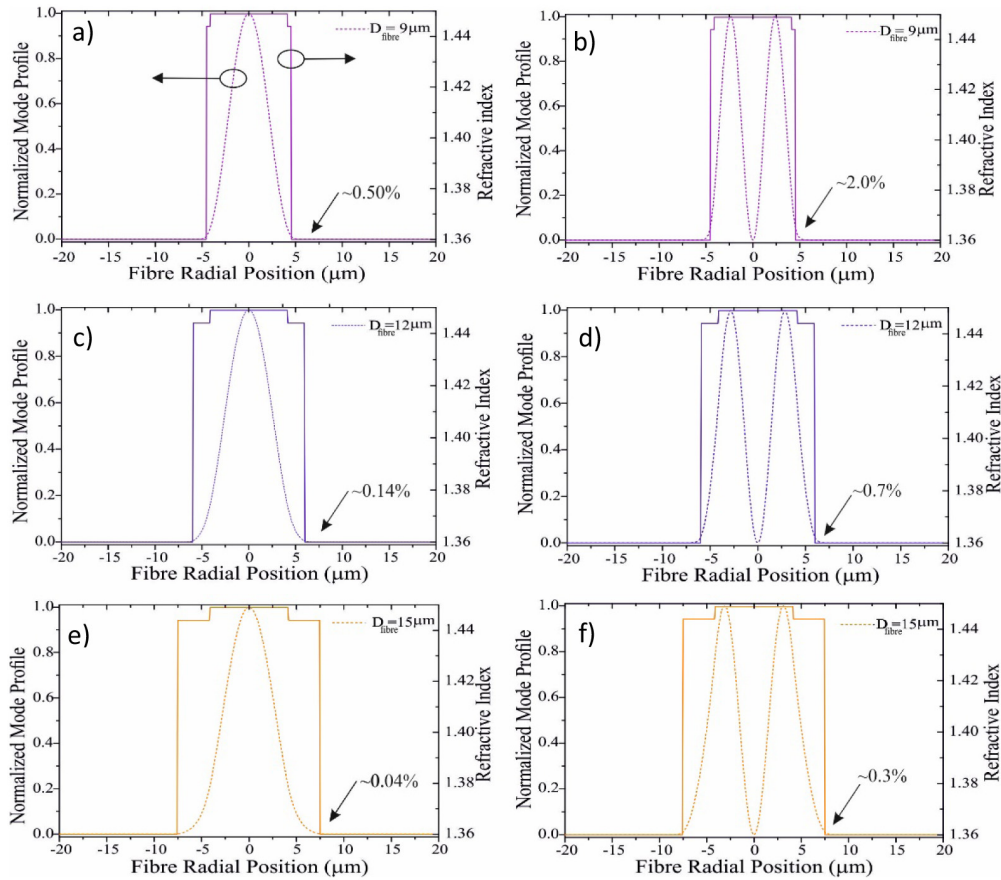


Fig. 2. The propagating mode profile of a progressively etched standard optical fibre, SMF28, and its refractive index profile for different diameters; $D_{\text{fibre}} = 9.0 \mu\text{m}$, $12.0 \mu\text{m}$, and $15.0 \mu\text{m}$ in BHF acid ($n = 1.360$ to be demonstrated below) for the fundamental mode LP01 a), c), e), and the first-higher-order mode LP11 b), d), f) at $\lambda = 1550.0 \text{nm}$.

The COMSOL model used here is based on solving the wave equation to analyse the mode field extent in a multi-layered cladding fibre consisting of a fused silica inner-cladding of varying thickness but fixed refractive index, and an outer-cladding of varying refractive index. For this analysis we are using a wavelength of 1550.0nm in the model. The FMP of the evanescent field extending into the outer-cladding, $\Gamma_{\text{outer-cladding}}$, is found via,

$$\Gamma_{\text{outer-cladding}} = 1 - (\Gamma_{\text{core}} + \Gamma_{\text{inner-cladding}}) \quad (5)$$

where Γ_{core} and $\Gamma_{\text{inner-cladding}}$ are the FMP values for the core and the inner-cladding, respectively. Figure 3(a), 3(b), 3(c), 3(d) shows $\Gamma_{\text{outer-cladding}}$ for the fundamental mode LP01, and higher-order modes LP11, LP02, LP21 against overall fibre diameter for different values of refractive index of the outer-cladding. As expected for refractive indices lower than the fused silica index, the FMP of the LP01 mode in the outer-cladding increases with a thinning inner-cladding. For example, for an outer-cladding refractive index of $n = 1.360$ (also manifested in Fig. 2(a) and 2(e)), and fibre diameter of $D_{\text{fibre}} = 15.0 \mu\text{m}$ the FMP is $\sim 0.04\%$, while for a fibre diameter of $D_{\text{fibre}} = 9.0 \mu\text{m}$ the FMP increases to $\sim 0.50\%$ for the same outer cladding refractive indices. Similarly, for a given diameter, e.g. $D_{\text{fibre}} = 9.0 \mu\text{m}$, an increase of the refractive index in the outer cladding will cause the FMP of the LP01 mode to increase as shown in Fig. 3(a).

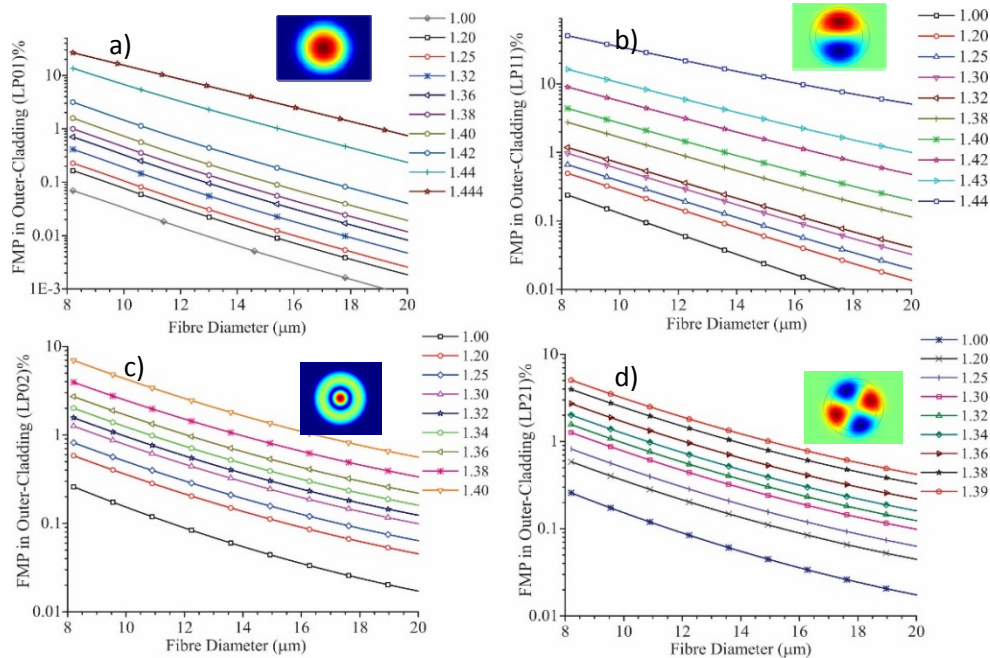


Fig. 3. Fraction of model power (FMP) in the outer-cladding as a function of different fibre diameters and various refractive indices of the surrounding region for; a) LP01. b) LP11. c) LP02. d) LP21 @ $\lambda = 1550.0\text{nm}$.

A similar trend is seen for the higher-order modes as illustrated in Fig. 3(b), 3(c) and 3(d). E.g. the FMP of the LP11 mode in the fibre with a diameter of $D_{\text{fibre}} = 9.5\mu\text{m}$ for $n = 1.320$ and 1.440 is 0.90% and 40.0% , respectively.

4. Experimental work and analysis results

To demonstrate this concept a series of controlled experiments were carried out. The schematic setup of the experiment is illustrated in Fig. 4. Several experiments were done using 8-10mm long uniform FBGs UV-written in single mode fibre, SMF28, with initial wavelengths of; 1534.5nm , 1544.0nm , and 1560.0nm respectively. The Bragg gratings had bandwidths of around 0.2nm with transmission losses of $\sim 5.5\text{dB}$ for the FBGs with $\lambda_B = 1534.5\text{nm}$ and 1544.0nm respectively, and a bandwidth around 0.8nm and transmission loss of $\sim 20\text{dB}$ for the FBG with $\lambda_B = 1560.0\text{nm}$. The gratings were mounted in a Teflon/Plastic container before being immersed in the BHF acid solution. Following the mounting the etching process was carried out under controlled environmental conditions of temperature ($T = 20^\circ\text{C} \pm 0.5^\circ\text{C}$) and relative humidity ($45\% \pm 5\%$). The reflection and transmission spectra of the gratings were monitored in real-time using a broadband source, and an optical spectrum analyser (OSA) (Agilent 86140B) with a nominal resolution bandwidth of 0.06nm . To substantiate the method under different wet etching conditions two different concentrations of BHF, (20:1) and (7:1), were applied for the etching processes in separate experiments.

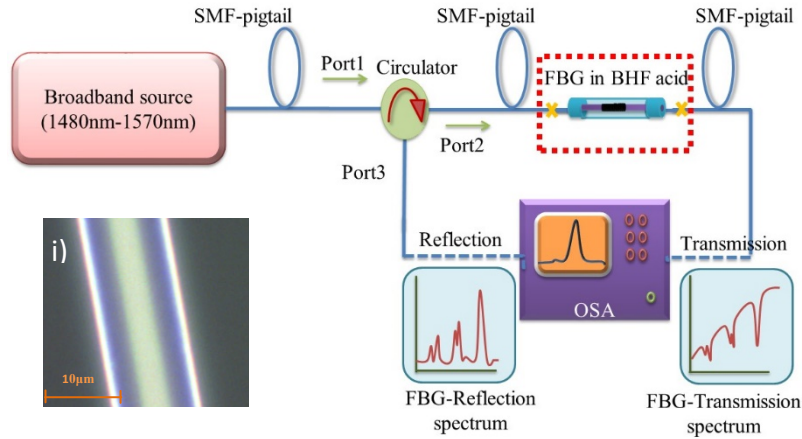


Fig. 4. Schematic of the experimental setup. (insert i) Microscope image of an etched uniform FBG with diameter $D_{\text{fibre}} \sim 11.0 \pm 0.2\mu\text{m}$.

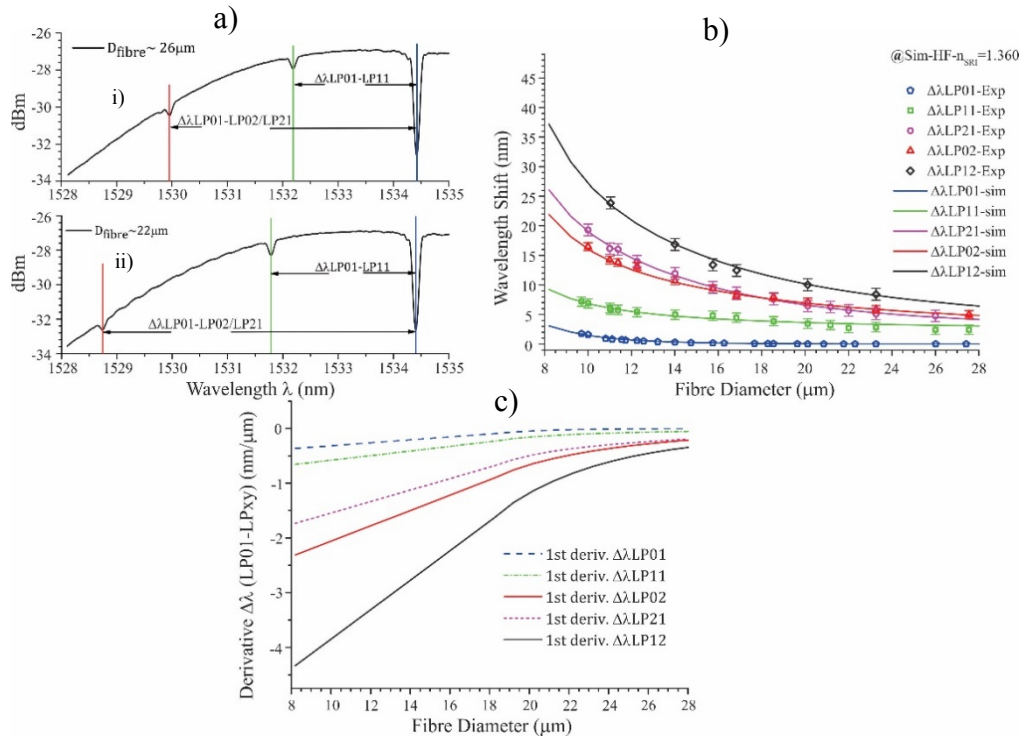


Fig. 5. a) i,ii) Transmission spectra of uniform FBG, measured in situ, during etching at two different stages of the etching process, and estimated etched FBG diameters of $D_{\text{fibre}} \sim 26\mu\text{m}$ and $22\mu\text{m}$ (based on an etch-rate estimate of $4.5\mu\text{m}/\text{hour}$). b) Measured (symbols) and simulated (solid-lines) results of the wavelength shifts, $\Delta\lambda_{\text{LPxy}}$, against fibre diameter for the fundamental and higher-order modes Bragg grating resonances using BHF (20:1) acid solution at $\lambda_B = 1550.0\text{nm}$. c) The first derivative of relative shifts of the higher-order modes and fundamental mode ($\Delta\lambda_{\text{LP01-LPxy}}$) as a function of fibre diameter.

4.1 Determination of the refractive index of 20:1 and 7:1 BHF solutions

When the etching fibre approach a diameter of $\sim 28\mu\text{m}$, several Bragg grating resonances, including those from the first higher-order modes, LP11 and the LP02/LP21 group, appear in addition to the LP01 mode Bragg resonance [Fig. 5(a)]. These higher order mode Bragg resonances appear at $\lambda_B^{LP11} = 1532.2\text{nm}$ and $\lambda_B^{LP02/LP21} = 1529.9\text{nm}$ as shown in Fig. 5(a) for an estimated fibre diameter of $D_{\text{fibre}} \sim 26\mu\text{m}$ based on estimated etch-rate of $4.5\mu\text{m}/\text{hour}$ for the 20:1 BHF solution. This diameter is reached after approximately 22 hours of etching. After a further ~ 1 hour of etching, the two groups of higher-order mode Bragg resonances have shifted to $\lambda_B^{LP11} = 1531.8\text{nm}$ and $\lambda_B^{LP02/LP21} = 1528.7\text{nm}$, respectively, whilst the LP01 mode Bragg grating resonance remain unchanged at $\lambda_B^{LP11} = 1534.4\text{nm}$. Evidently there is a relatively large wavelength shift between the higher-order mode resonances and the LP01 mode resonance for a reduction of the fibre diameter of $\sim 4\mu\text{m}$, increasing the differential wavelength shifts between the LP01 and higher-order mode Bragg resonances from $\Delta\lambda_{(LP01-LP11)} = 2.4\text{nm}$ and $\Delta\lambda_{(LP01-LP02/LP21)} = 4.5\text{nm}$, to $\Delta\lambda_{(LP01-LP11)} = 2.6\text{nm}$ and $\Delta\lambda_{(LP01-LP02/LP21)} = 5.7\text{nm}$ for a fibre diameter of $\sim 26\mu\text{m}$ and $\sim 22\mu\text{m}$, respectively. As expected from the less confined LP02/LP21 mode group, the Bragg resonances from these modes show a larger wavelength shift against the thinning cladding, Fig. 5c. The etching was continued until an estimated target diameter of $D_{\text{fibre}} \sim 11.0\mu\text{m}$ was reached. At the completion of the etch, and whilst the fibre was still in the BHF acid, the observed Bragg wavelength shifts of the LP01, LP11, LP02, LP21 mode Bragg resonances relative to the LP01 mode Bragg wavelength of the un-etched fibre were, -1.0nm , -6.1nm , -14.2nm , and -16.2nm , respectively. As mentioned above, the initial etch-rate of $4.5\mu\text{m}/\text{hour}$ for the 20:1 BHF acid solution was used for this target diameter estimate, however since this etch-rate is strongly dependent on the temperature and humidity conditions during the etching process it is difficult to predict the exact value of the final fibre diameter. Following the completion of the etch process the FBG was removed from the etching container and rinsed thoroughly in deionised water. To corroborate these measurements a second FBG with an initial Bragg wavelength of 1560.0nm also written in SMF28 fibre was etched in the same 20:1 BHF solution. In this case the target diameter was $\sim 10.0\mu\text{m}$. The emergence of higher order mode Bragg resonances were again observed for fibre diameters below $\sim 28\mu\text{m}$, and at the end of the etch the observed Bragg wavelength shifts of the LP01, LP11, LP02, LP21 mode resonances relative to the LP01 mode Bragg wavelength of the un-etched fibre were; -1.6nm , -6.9nm , -16.5nm , and -19.3nm , respectively. Within the measurement precision of the OSA these values are very well matched with the numerical simulations for a refractive index of 1.360, as shown in Fig. 5(b) and 5(c).

To calibrate the concept, the two etched FBGs ($D_{\text{fibre}} \sim 11.0\mu\text{m}$ and $10.0\mu\text{m}$) were immersed in a range of different liquids of well-known refractive index, n , @ 1550nm [24]. These included, water $n = 1.318$, methanol $n = 1.317$, acetone $n = 1.350$, ethanol $n = 1.352$, isopropanol $n = 1.374$ and ethylene glycol $n = 1.420$. The resulting wavelength shifts of the fundamental mode Bragg resonance are shown in Fig. 6(a), and the relative wavelength shifts $\Delta\lambda_{(LP01-LP11)}$ between the LP01 and LP11 mode Bragg resonances are shown in Fig. 6(b). These results were subsequently compared with the wavelength shifts observed at the end of the etch process when the etched FBG was still submerged in the 20:1 BHF solution. As indicated in the figures this suggests a refractive index of the 20:1 BHF solution of 1.360 ± 0.005 . Following the completion of the calibration measurements the diameter of the etched fibres were measured with a microscope to validate their diameter.

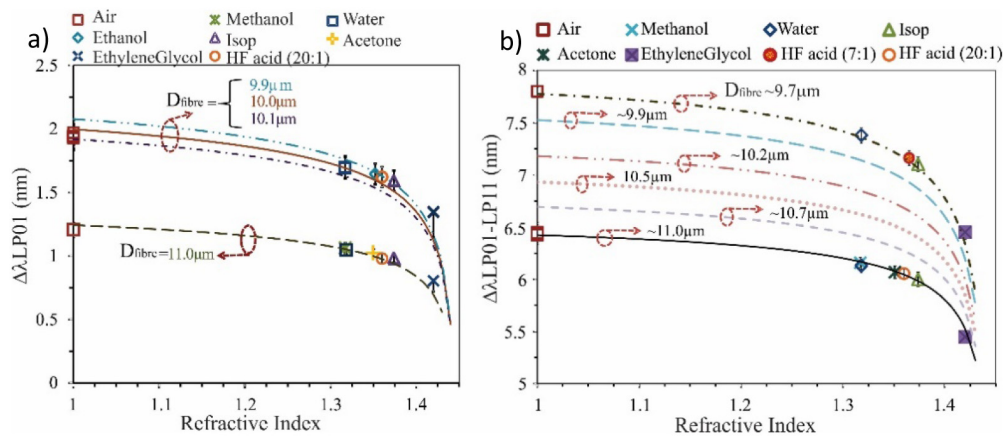


Fig. 6. Measured (symbols) and simulated (lines) results of relative wavelength shifts of; a) LP01 mode at $\lambda_B^{LP01} = 1534.4\text{nm}$ and 1560.0nm with $D_{\text{fibre}} = 11.0\mu\text{m}$ and $10.0\mu\text{m}$, respectively, using (20:1) BHF acid solution. b) LP11 mode at $\lambda_B^{LP01} = 1534.4\text{nm}$ (solid line) and $\lambda_B^{LP01} = 1544.0\text{nm}$ (dashed lines), against different external refractive indices applied on etched FBG with $D_{\text{fibre}} = 11.0\mu\text{m}$ using (20:1) BHF acid and $D_{\text{fibre}} = 9.7\mu\text{m}$ using (7:1) BHF acid.

To validate the concept further we also carried out the etching experiment on an FBG using a 7:1 BHF acid solution. In this case the FBG had an initial fundamental mode Bragg resonance of 1544.0nm . The nominal etch-rate of fused silica with a 7:1 BHF acid solution is $\sim 12\mu\text{m}/\text{hour}$, so being able to precisely terminate the etch process at the correct time becomes even more critical to achieve a specific diameter target. In this case the etch process was completed when the diameter had reached an estimated value of $9.7\mu\text{m}$ subsequently confirmed to be $\sim 10\mu\text{m}$ when measured using a microscope. The etched FBG was calibrated using the procedure mentioned above, and in this case the LP01 and LP11 mode Bragg resonances showed relative wavelength shifts for the same range of materials mentioned above with resulting values plotted in Fig. 6(b). Using this analysis we were able to estimate the refractive index of the 7:1 BHF acid solution to be 1.370 ± 0.005 . From Fig. 6(a) we estimate the refractive index sensitivity for the fundamental mode and first higher-order mode for fibre diameters of $10\mu\text{m}$ and $11\mu\text{m}$ to be $1.21\text{nm}/\text{RIU}$ and $1.97\text{nm}/\text{RIU}$ respectively, in the range $1.32 - 1.38$. This corresponds well with values reported in literature for similar fibres of similar diameters [23,25].

A key point in our work, and the main difference from these earlier works, is the precision with which we can claim the actual fibre diameter referring to these sensitivity values. The main limitation to how accurately the final diameter of the etched fibre can be predicted is mostly down to the resolution of the spectrometer used to measure the Bragg resonances of the different mode orders. There is also a small limitation resulting from the time it takes to terminate the etch-process, but that is largely down to the concentration of the BHF acid solution used. E.g. the 20:1 BHF solution used in some of this work has, as also mentioned above, a room temperature etch-rate of SiO_2 of $4.5\mu\text{m}/\text{hour}$, or $1.25\text{nm}/\text{s}$. Assuming it takes 15-20 seconds to terminate the etch and completely rinse the etched fibre for HF acid in DI water to arrest the etch process, the precision would be $\sim 20\text{nm}$ or $0.02\mu\text{m}$. For the 7:1 BHF solution utilised a similar argument can be used to estimate the ultimate precision. As mentioned above this work used an OSA as the spectrometer with a resolution bandwidth of 0.06nm . There are plenty faster spectrometers and interrogators available, such as, for example, the I-Mon interrogation monitor series from Ibsen Photonics [26]. Fast measurement (10's of kHz) of the Bragg resonances is therefore possible allowing for 'real-time' measurements. There are also Bragg resonance peak-tracking algorithms, such as the Karhunen-Loeve Transform (KLT), that can provide dramatic improvements to the spectral

resolution and determination of the precise Bragg resonances even when using relatively coarse initial spectral resolution. Spectral accuracy values as low as 0.22pm employing KLT have been reported combined with fast operation typically in the kHz regime [27]. In this work we estimate a precision of $\pm 200\text{nm}$ in determining the fibre diameter because of the resolution bandwidth and scanning speed of the spectrometer (OSA) used to monitor the Bragg resonances, but even higher precision should be possible if applying any of the above mentioned techniques during the monitoring of the etch process.

It is worth noting that the principle of the technique presented here not is limited to silica fibres. In principle it is applicable to any fibre and waveguide material including for example polymer waveguides and soft-glass waveguides. E.g. polymer optical fibres (POFs) [28] are typically etched using acetone or other solvents with well-known refractive index. For the technique to work it is only necessary that the refractive index of the material used for the etching process is lower than that of the waveguide material itself. In the case of most commonly used materials in POFs, acetone fulfils this requirement. That therefore implies that it is possible to monitor any shift in the generated Bragg resonances in situ during the etching process so it can be terminated when the diameter has reached the desired value.

5. Conclusion

A technique to determine, in real-time, the diameter of a fibre being etched is presented. By monitoring the differential wavelength shifts between the fundamental mode and first higher-order mode Bragg resonances in short fibre Bragg gratings, we show that it is possible to determine the fibre diameter with a precision of $\sim 200\text{nm}$ for diameters below $\sim 25\mu\text{m}$. In this work we demonstrate the technique on a standard single-mode silica fibre etched in hydrofluoric acid, but also highlight that the concept should be applicable to optical fibres made in other materials as well such as for example polymer.

References

1. K. O. Hill and G. Meltz, "Fiber Bragg grating technology fundamentals and overview," *J. Lightwave Technol.* **15**(8), 1263–1276 (1997).
2. M. A. Davis and A. D. Kersey, "Fiber Bragg grating sensors for infrastructure sensing," in *Optical Fiber Communication Conference, OSA Technical Digest Series* (Optical Society of America, 1997), paper WL15.
3. A. Othonos and K. Kalli, *Fiber Bragg Gratings: Fundamentals and Applications in Telecommunications and Sensing* (Artech House Boston, 1999).
4. A. Iadicicco, S. Campopiano, A. Cutolo, M. Giordano, and A. Cusano, "Microstructured fibre Bragg gratings: analysis and fabrication," *Electron. Lett.* **41**(8), 466–468 (2005).
5. R. Kashyap, *Fiber Bragg gratings*, 1st ed. (Academic Press, 1999).
6. B. Lee, "Review of the present status of optical fiber sensors," *J. Optical Fiber Technology* **9**(2), 57–79 (2003).
7. B.-O. Guan, H.-Y. Tam, X.-M. Tao, and X.-Y. Dong, "Simultaneous strain and temperature measurement using a superstructure fiber Bragg grating," *IEEE Photonics Technol. Lett.* **12**(6), 675–677 (2000).
8. S. J. Mihailov, "Fiber Bragg grating sensors for harsh environments," *Sensors (Basel)* **12**(2), 1898–1918 (2012).
9. B. Zhang and M. Kahrizi, "High-temperature resistance fiber Bragg grating temperature sensor fabrication," *IEEE Sens. J.* **7**(4), 586–591 (2007).
10. A. Iadicicco, A. Cusano, S. Campopiano, A. Cutolo, and M. Giordano, "Thinned fiber Bragg gratings as refractive index sensors," *IEEE Sens. J.* **5**(6), 1288–1295 (2005).
11. S. Sridevi, K. S. Vasu, N. Jayaraman, S. Asokan, and A. K. Sood, "Optical bio-sensing devices based on etched fiber Bragg gratings coated with carbon nanotubes and graphene oxide along with a specific dendrimer," *Sens. Actuators B Chem.* **195**, 150–155 (2014).
12. B.-b. Luo, X.-j. Zhou, M.-f. Zhao, N.-b. Zhong, and S.-f. Wang, "Recent developments in microstructured fiber Bragg grating refractive index sensors," *J. Photonics Energy* **1**(1), 1–12 (018002) (2010).
13. B. N. Shivananju, M. Renilkumar, G. R. Prashanth, S. Asokan, and M. M. Varma, "Detection limit of etched fiber Bragg grating sensors," *J. Lightwave Technol.* **31**(14), 2441–2447 (2013).
14. A. Iadicicco, S. Campopiano, A. Cutolo, M. Giordano, and A. Cusano, "Refractive index sensor based on microstructured fiber Bragg grating," *IEEE Photonics Technol. Lett.* **17**(6), 1250–1252 (2005).
15. Y. Wu, B. Yao, A. Zhang, Y. Rao, Z. Wang, Y. Cheng, Y. Gong, W. Zhang, Y. Chen, and K. S. Chiang, "Graphene-coated microfiber Bragg grating for high-sensitivity gas sensing," *Opt. Lett.* **39**(5), 1235–1237 (2014).

16. B. Shivananju, M. Varma, S. Asokan, S. Yamdagni, R. Fazuldeen, and S. Nithin, "Highly sensitive carbon nanotubes coated etched fiber Bragg grating sensor for humidity sensing," *IEEE Sens. J.* **14**(8), 2615–2619 (2014).
17. Y. Wu, B.-C. Yao, Y. Cheng, Y.-J. Rao, Y. Gong, W. Zhang, Z. Wang, and Y. Chen, "Hybrid graphene-microfiber waveguide for chemical gas sensing," *IEEE J. Sel. Top. Quantum Electron.* **20**(1), 49–54 (2014).
18. K. T. Dinh, Y.-W. Song, S. Yamashita, and S. Y. Set, "Realization of all-fiber tunable filter & high optical power blocker using thinned fiber Bragg gratings coated with carbon nanotubes," in *Optical Fiber Communication Conference and Exposition and The National Fiber Optic Engineers Conference*, OSA Technical Digest Series (Optical Society of America, 2007), paper OWG5.
19. D. F. Penning, D. Weimer, and W. F. Rumpel, "Indices of refraction of HF and F2. II," *J. Chem. Phys.* **59**(5), 2496–2497 (1973).
20. D. L. Drummond, "Refractive index of HF from 2.5 μm to 2.9 μm ," *Appl. Opt.* **21**(23), 4331–4334 (1982).
21. A. Chryssis, S. Saini, S. Lee, and M. Dagenais, "Increased sensitivity and parametric discrimination using higher order modes of etched-core fiber Bragg grating sensors," *IEEE Photonics Technol. Lett.* **18**(1), 178–180 (2006).
22. M. Monerie, "Propagation in doubly clad single-mode fibers," *IEEE J. Quantum Electron.* **18**(4), 535–542 (1982).
23. A. N. Chryssis, S. M. Lee, S. B. Lee, S. S. Saini, and M. Dagenais, "High sensitivity evanescent field fiber Bragg grating sensor," *IEEE Photonics Technol. Lett.* **17**(6), 1253–1255 (2005).
24. "Refractive index database", <https://refractiveindex.info/>
25. D. A. Pereira, O. Frazão, and J. L. Santos, "Fiber Bragg grating sensing system for simultaneous measurement of salinity and temperature," *Opt. Eng.* **43**(2), 299–304 (2004).
26. Ibsen Photonics, <https://ibsen.com/products/interrogation-monitors/>
27. D. Tosi, "Review and analysis of peak tracking techniques for fiber Bragg grating sensors," *Sensors (Basel)* **17**(10), 2368–2402 (2017).
28. G. Rajan, K. Bhowmik, J. Xi, and G.-D. Peng, "Etched polymer fibre Bragg gratings and their biomedical sensing applications," *Sensors (Basel)* **17**(10), 2336–2348 (2017).